Protective properties of warp-knitted spacer fabrics under impact in hemispherical form. Part I: Impact behavior analysis of a typical spacer fabric

Yanping Liu, Wai Man Au and Hong Hu

Textile Research Journal 2014 84: 422 originally published online 9 August 2013
DOI: 10.1177/0040517513495941

Original article

Textile Research Journal

Textile Research Journal
2014, Vol. 84(4) 422–434

DOI: 10.1177/0040517513495941
trj.sagepub.com
SAGE

Protective properties of warp-knitted spacer fabrics under impact in hemispherical form. Part I: Impact behavior analysis of a typical spacer fabric

Yanping Liu, Wai Man Au and Hong Hu

Abstract

This paper presents an experimental study of the protective properties of warp-knitted spacer fabrics developed for protecting the human body on impact. A drop-weight impact tester was used to test the fabrics in a hemispherical form to simulate the use of impact protectors in real life. The study consists of two parts. The first part, presented in the current paper, focuses on the impact behavior of a typical spacer fabric impacted at different levels of energy. The analysis includes the impact process and the energy absorption and force attenuation properties of the spacer fabric. Frequency domain analysis is also used, to identify the different deformation and damage modes of the fabric under various levels of impact energy. The results show that the impact behavior of the fabric under impact in the hemispherical form is different from that in the planar form. The results also indicate that the curvature of the fabric can reduce energy absorption during the impact process and therefore reduce the force attenuation properties of the spacer fabric. This study provides a better understanding of the protective properties of spacer fabrics. The effect of fabric structural parameters and lamination on the protective properties of spacer fabrics under impact will be presented in Part II.

Keywords

spacer fabric, impact protection, energy absorption, transmitted force

Over the past few decades a wide range of personnel protective equipment (PPE) has been developed to protect wearers from various types of risks or hazards to their health and safety.[1–7] Impact protectors, which are the most commonly used PPE, are normally manufactured to include energy-absorbing material in the form of pads.[8,9] They are integrated or inserted into protective clothing or equipment specially designed for protecting the human body from impact, blows or falls. A number of different types of impact protectors are on the market for protecting different areas of the body in a variety of circumstances.[1–4]

To ensure adequate protection is provided for the intended use a series of standard tests have been developed for evaluating the protective performance of commercial impact protectors for a variety of sporting applications. For instance, European Standards BS EN 13546, 13277–1, 13158, 13567, 14120, 13061, 1621–1, 1621–2 and British Standard BS 6183–3 specify the requirements and test methods for hand, arm, leg, foot, instep, shin, chest, abdomen, genitals, trunk, head, breast and shoulder protectors for field hockey, martial arts, equestrianism, fencing, roller sports, football, motorcycling and cricket. In these standards impact protection is generally measured by the force transmitted during impact; a striker of specified shape, size and weight drops freely onto the protector placed on a hemispherical anvil with the required velocity and impact energy. The hemispherical anvils have different curvatures to simulate the areas of the body to be protected. The radius of the anvils ranges from 12.5

Institute of Textiles and Clothing, Hong Kong Polytechnic University, Hung Hom, Kowloon, Hong Kong, China

Corresponding author:
Hong Hu, Institute of Textiles and Clothing, Hong Kong Polytechnic University, Hung Hom, Kowloon, Hong Kong, China.
Email: tchuhong@polyu.edu.hk

to 150 mm, and the impact energies for the various types of protector lie between 1 and 60 J. Among these standards the two European Standards for motorcyclists' impact protectors are those most commonly quoted for evaluating protective performance, one for limbs and shoulders (BS EN 1621–1:1998) and the other for back protection (BS EN 1621–2:2003). Under the European directive on personal protective equipment any clothing claiming to provide protection from injury must be tested and labeled that it complies with the relevant standard.

The use of warp-knitted spacer fabrics in clothing and equipment providing protection against impact has attracted great attention in recent years due to their combination of protection and comfort in use. The static and dynamic compression behavior of a series of warp-knitted spacer fabrics has been investigated in our previous studies,[10,11] and the energy absorption performance and force attenuation capability of these fabrics under flatwise static and impact compression has been analyzed in detail. These studies indicate that these fabrics have the key feature of behaving as cushioning materials, providing three distinct stages in static and dynamic compression, described as linear elasticity, plateau and densification. However, in order to offer an adequate combination of protection and comfort, the protective material must conform to the shape and curvature of the body part being protected. There is no doubt that the impact properties of a protective material of curved shape are different from those of a planar shape, due to the change in boundary conditions during loading. Most recently, Guo et al. have reported an experimental investigation into the impact behavior of warp-knitted spacer fabrics of hemispherical shape.[12] The impact energy and weight of the striker were kept constant, and only the contact forces were measured. The tests were quoted as having been carried out according to European Standard BS EN 1621–1:1998. However, this standard specifies that protectors should be impacted using a striker of 5 kg weight at a kinetic energy of 50 J, and the transmitted forces then measured. Furthermore, their study did not pay attention to the relationship between energy absorption capacity and force attenuation properties, which is very important in designing fabrics to satisfy protective requirements.

The present paper describes our assessment of the protective properties of warp-knitted spacer fabrics obtained from impact tests conducted strictly in accordance with European Standard BS EN 1621–1:1998 in hemispherical form, in order to simulate the realistic requirements of human body protection. The study is in two parts. Part I focuses on the analysis of the impact behavior of a typical spacer fabric in order to understand the impact process, energy absorption and force attenuation mechanism of the spacer fabric. Later, Part II will discuss the effect of structural parameters and lamination on the impact protective performance of the fabrics. It is expected that this study will provide a deeper understanding of the impact properties of warp-knitted spacer fabrics for protection of the human body.

Experimental details

Spacer fabric

As shown in Figure 1, a typical warp-knitted spacer fabric sample was used in the analysis of impact behavior. The fabric was knitted on a GE296 (RD6) E18 high-speed double needle bar Raschel machine with six yarn guide bars (GB). A polyester multifilament of 300 denier and 96 filaments (300D/96F) was used to create the binding of the structure during the knitting process, through GB1, GB2 for the top outer layer and GB5, GB6 for the bottom outer layer with full threading. A polyester monofilament 0.2 mm in diameter (fineness 400 denier) was used as a spacer yarn to connect the two outer layers through GB3 and GB4 with 1 full and 1 empty threading. The chain notation and the yarns used for each yarn guide bar are listed in Table 1, and details of the fabric are summarized in Table 2. The fabric thickness was measured using a digital thickness tester (SDL Atlas M034e).

Test method

The impact tests were conducted on a drop-weight impact tester, specially designed and manufactured by the King Design Company in Taiwan, in strict accordance with European Standard BS EN 1621–1:1998. As shown in Figure 2, the striker is released and drops down a vertically guided path onto the sample located on the anvil. The center of mass of the falling block lies above the center of the anvil. The striker is constructed of polished steel, with a weight of 5 kg and a face size 40 mm × 80 mm with 5 mm radius edges. The impact energy can be controlled by changing the dropping height of the striker. The anvil is also made of polished steel, with a total height of 170 mm and a hemispherical surface of radius 50 mm, to simulate the curvature of human shoulder, elbow, knee, forearm, tibia or hip. The hemispherical anvil was mounted on a massive base (1000 kg) through a load cell (1210AF–50KN from Interface Inc. in USA, with a sensitivity of 4.171 mV/V) in line with its sensitivity axis, to measure the transmitted force. In addition, in order to obtain more information during the impact process, the acceleration of the striker was measured by means of

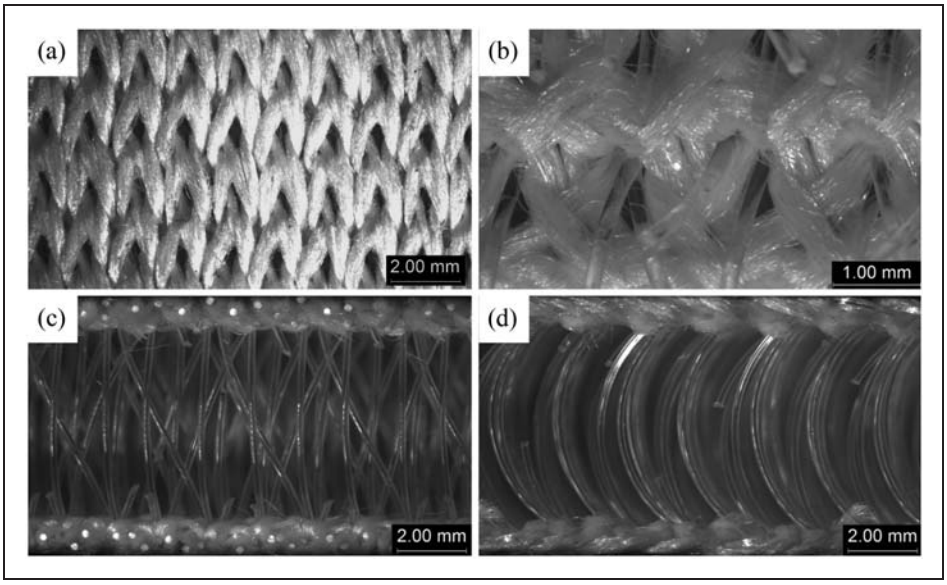

Figure 1. Photographs of the spacer fabric sample: (a) outer surface view; (b) inner surface view; (c) cross-section view from the wale direction; (d) cross-section view from the course direction.

Table 1. Chain notation and yarns used for the spacer fabric

Layers	Guide bars	Chain notation	Threading	Yarn
Top layer	GB1	1–0 0–0/3–2 3–3//	Full	300D/96F polyester DTY
	GB2	2–1 1–1/1–0 0–0//	Full	300D/96F polyester DTY
Spacer layer	GB3	1–0 3–2/3–2 1–0//	1 full 1 empty	0.2 mm polyester monofilament
	GB4	3–2 1–0/1–0 3–2//	1 full 1 empty	0.2 mm polyester monofilament
Bottom layer	GB5	0–0 2–1/1–1 1–0//	Full	300D/96F polyester DTY
	GB6	3–3 1–0/0–0 3–2//	Full	300D/96F polyester DTY

Table 2. Details of the spacer fabric sample

Thickness (mm)	Areal density (g/m^2)	Bulk density (kg/m^3)	Stitches per cm^2
7.52 ± 0.06	1008.29 ± 10.68	134.08 ± 1.42	41.15

accelerometers glued or screwed to it. The acceleration readings obtained were used for deriving the displacement of the striker (or the compression depth of the fabric) and the contact forces between striker and fabric. Three accelerometers were used, corresponding to the degree of the resultant acceleration of the striker. Two were Isotron accelerometers from Endevco Company (USA), Model 2250AM1–10 (sensitivity 9.929 mV/g with a measuring range of ±500 g) and Model 25B (sensitivity 4.550 mV/g and measuring range ±1000 g). These were glued to the striker for the impact tests. The third was a Model 8704B5000 K–SHEAR accelerometer (sensitivity 0.976 mV/g and measuring range ±5000 g) from Kistler Instrumente, Winterthur, Switzerland. This was screwed to the striker for the impact tests. Two identical charge amplifiers (Interface, Scottsdale, AZ, USA) were used to amplify the voltage of the impact signals. Signals from the charge amplifiers were recorded through two channels at 10^5 Hz, Channel 1 as the triggered channel for the transmitted force, and Channel 2 for the acceleration. A high-speed data capture card NI6040E (PCI Bus) was employed to record both the transmitted force and the acceleration.

The specimens are conformed onto the anvil using a ring fixture as shown in Figure 3. Elastic straps are angled downwards around the anvil to pull the

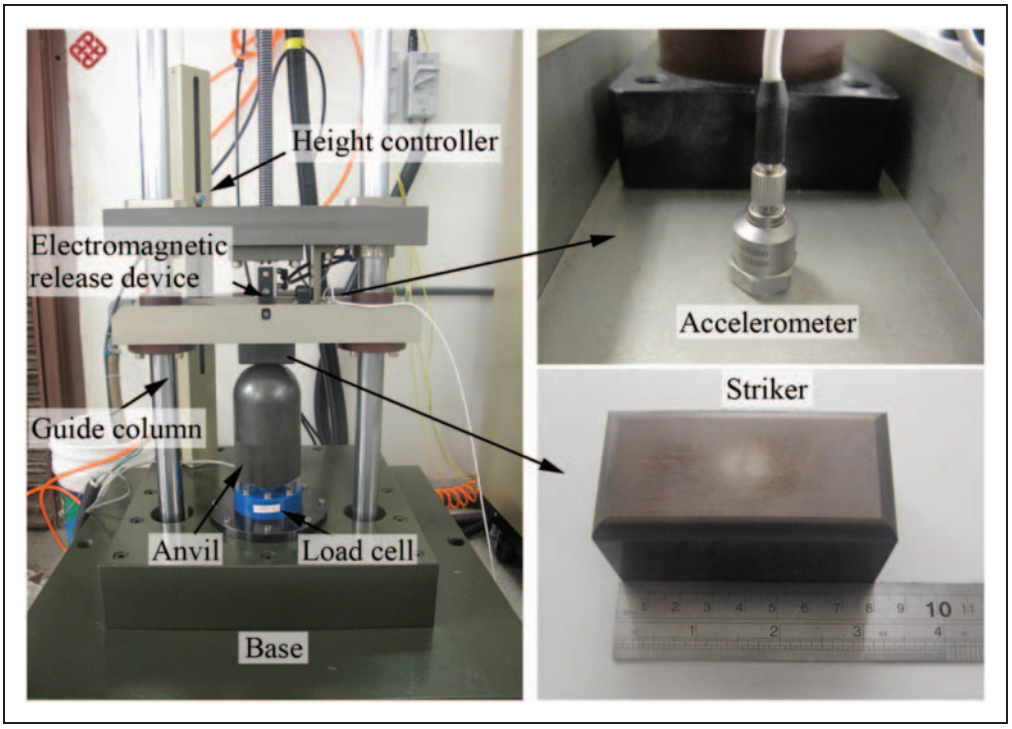

Figure 2. Drop-weight impact tester according to European Standard BS EN 1621–1:1998.

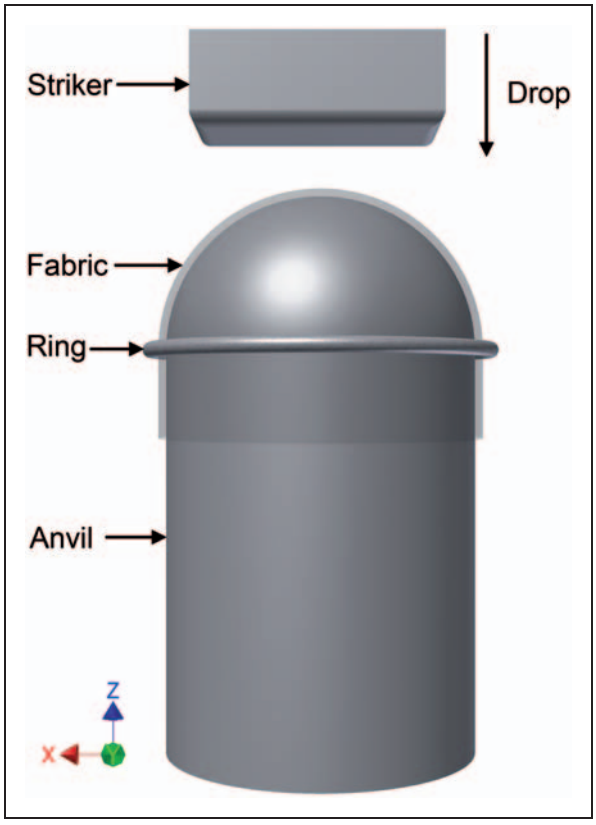

Figure 3. Schematic presentation of the impact test.

sample down to the anvil without significant additional compression of the sample. The straps are connected to a flat elastic ring surrounding the impact area without covering it. Since areas of the human body may in practice be subjected to different levels of energy impact in different sports or other activities, impact energies ranging from 1 to 60 J are required for testing impact protectors according to the standards mentioned. In order to obtain a full picture of the impact behavior of a typical warp-knitted spacer fabric under different levels of impact energy 5, 10, 20, 30, and 40 J were selected for the impact tests in the study, in addition to the 50 J specified in BS EN 1621–1:1998. All the tests were conducted at 20°C and 65% relative humidity. For each impact energy level, a total of 10 repeat tests were carried out to ensure consistency.

Results and discussion

Impact process analysis

Typical acceleration and transmitted force signals for different levels of impact energy are shown in Figure 4(a) and (b), respectively. Figure 4(a) shows that in the initial stage the acceleration gives a lower value over a relatively longer time, and then rapidly rises to a peak in the second stage. Under higher

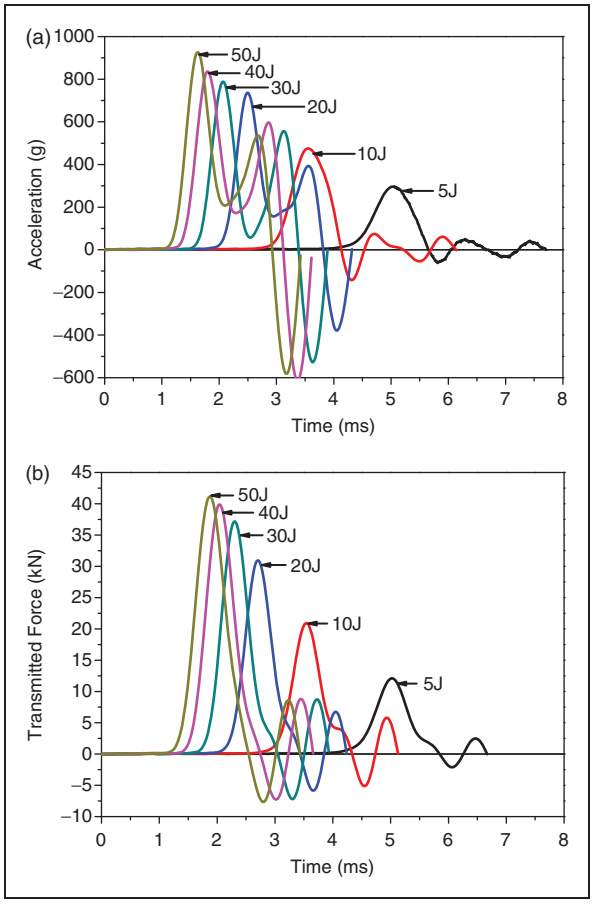

Figure 4. Impact signals at different energy levels: (a) acceleration, and (b) transmitted force.

energy impact a greater peak in acceleration response is obtained over a shorter time. According to the theorem of momentum, a shorter duration of impact will lead to a higher acceleration and a higher reactive force. In the absence of fabric the dropping striker is instantaneously stopped by the anvil, producing a very high acceleration and dynamic contact force. However, with the fabric located on the anvil surface the striker experiences deceleration as it strikes the fabric. During the deceleration the fabric first stores and dissipates the kinetic energy of the impact and then releases the stored energy over a longer duration, thereby leading to a reduction in the acceleration of the striker and generating a smaller contact force between the striker face and the upper surface of the fabric. It should be noted that the increase in impact energy will lead to an increase in the velocity of the striker at the beginning of its contact with the fabric. Due to the increase in the initial contact velocity, the time taken by the striker to compress the fabric to its denser state is shortened. Since the fabric has higher compression resistance in its densified state it is able to stop the striker more quickly, and at the peak point the increase in impact energy will therefore result

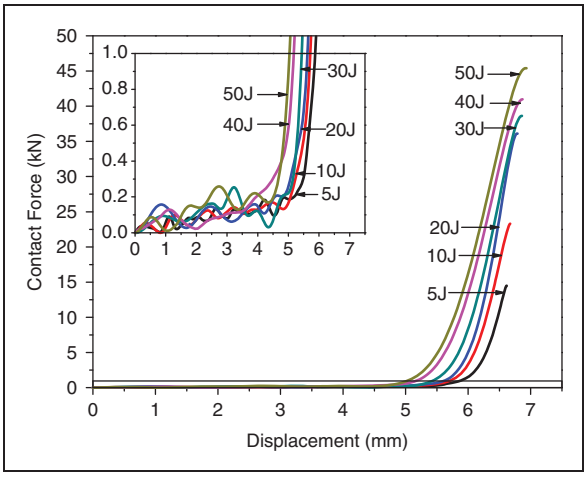

Figure 5. Contact force–displacement curves at different energy levels.

in a reduction in impact time and an increase in acceleration.

During the impact process, the force is transmitted to the anvil through the deformed fabric and the transmitted force curves therefore have a similar form to the acceleration curves shown in Figure 4(b). For a similar reason a higher level of impact energy will result in a greater transmitted peak force over a shorter duration.

The contact force–displacement curves are obtained by integrating the respective acceleration curves, as shown in Figure 5. Inset is a magnified view of the curves. Similar to the acceleration and transmitted force signals, two clear stages in the contact force can be observed, the first very slowly increasing and the second increasing rapidly. The slowly increasing stage of the curves is generally located in the displacement range below 5.5 mm, corresponding to a compression strain of 73%. Subsequently, as the displacement increases, the contact force increases rapidly. Figure 5 also shows that the curves are sensitive to strain rate. As the impact energy is controlled by the dropping height of the striker, the change in impact energy implies a change in initial contact velocity or strain rate. The spacer fabric is made up of polyester fibers with strain rate sensitivity, and its impact properties are therefore also sensitive to strain rate. Figure 5 indicates that a striker of higher kinetic energy can more quickly compress the fabric into its densification stage and with a larger final displacement. This is one of the reasons why the fabric has a higher peak contact force when it is impacted at higher kinetic energy.

It is interesting to compare the impact behavior of the same fabric impacted in different shapes. A previous study has shown that the force–displacement curve of the fabric under flatwise impact includes three main stages, linear elasticity, plateau and densification.[11]

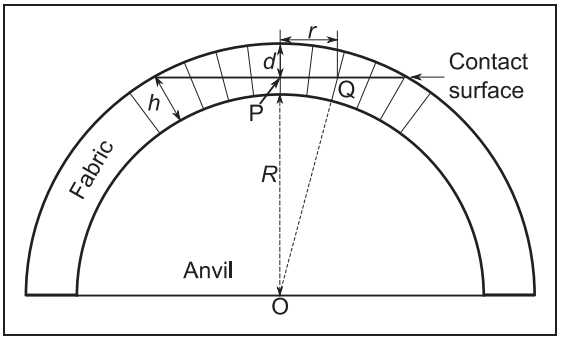

Figure 6. Cross-section of the fabric on the anvil.

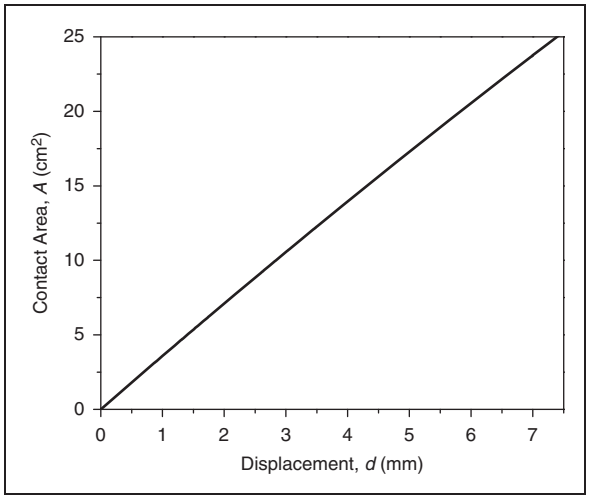

Figure 7. Variation in contact area with displacement of the striker.

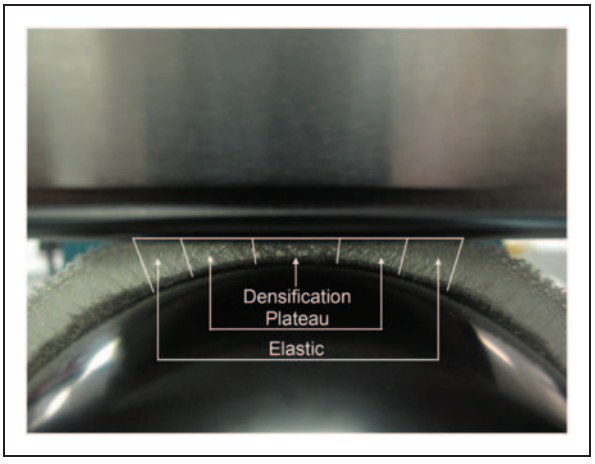

Figure 8. Different deformations of the spacer monofilaments within the fabric in the hemispherical form under impact.

However, the impact contact force–displacement curves of the spacer fabric in the hemispherical form show only two stages, as mentioned above, and no plateau stage is observed under hemispherical impact. This difference originates from the different boundary conditions of the spacer fabric in planar and hemispherical shapes. One reason is that, under flatwise impact, the contact area between the striker face and the fabric surface remains constant throughout the entire impact process. By contrast, the contact area for the fabric in the hemispherical form is changed during the impact process and increases with the displacement of the striker. This can be confirmed by the following geometrical analysis.

As shown in Figure 6, a cross-section of the fabric through the central axis of the anvil is used to derive the contact area between the striker face and the fabric surface during the impact, based on the axis-symmetrical property of the fabric shape and the anvil. Geometric analysis of Figure 6 gives the following relationship:

$$A = \pi\left[(R+h)^2-(R+h-d)^2\right], \qquad (1)$$

where A is the contact area, h is the fabric thickness, R is the anvil radius, and d is the displacement of the striker. In this study, R and h are equal to 50 mm and 7.52 mm, respectively. Using these values, the variation in contact area with the displacement of the striker is plotted in Figure 7. It can be seen that the contact area of the fabric with the striker rapidly increases as the displacement of the striker increases. As the contact area increases, the contact force cannot remain constant. Therefore, the plateau stage of the contact force–displacement curves obtained under the flatwise impact condition is not possible under a hemispherical-shaped impact.

Another reason for no plateau stage being observed under hemispherical impact is that the spacer monofilaments within the fabric deform in different ways under flatwise impact and under impact of the fabric in the hemispherical form. Under flatwise impact all the spacer monofilaments simultaneously withdraw the impact load and are subjected to the same deformation. On the other hand, in the hemispherical form the spacer monofilaments at different positions experience different deformations. As shown in Figure 8, when the displacement of the striker is larger than the densification displacement of the fabric obtained under flatwise impact, the linear elasticity, plateau and densification of the spacer monofilaments within the fabric can all be observed at the same time under the impact of the fabric in the hemispherical form. It can be seen that the closer the position of a spacer monofilament to the central axis of the anvil, the greater the deformation it experiences.

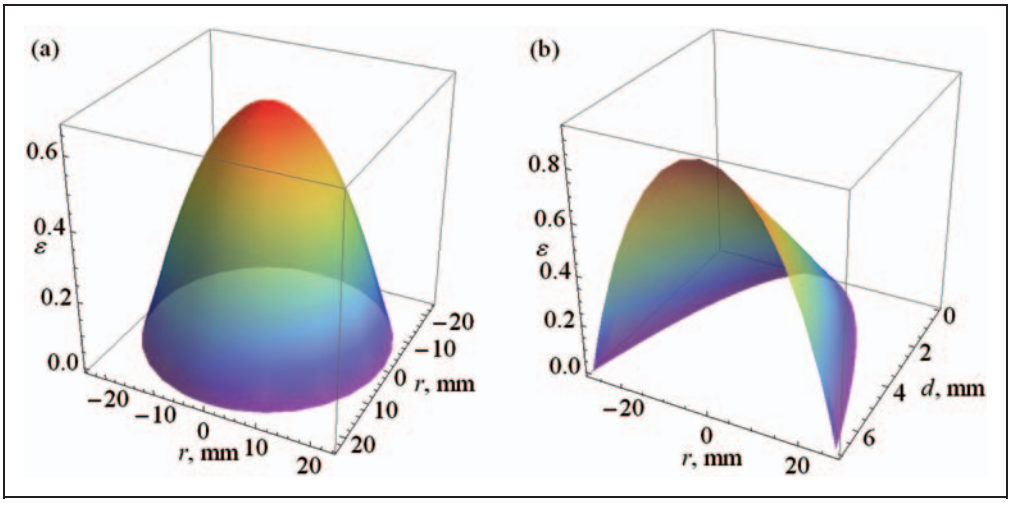

Figure 9. Distribution of strain ε with r: (a) for a given displacement of the striker $d = 5$ mm; (b) for varied values of d in the cross-section of the fabric.

With reference to Figure 6, the strain of a spacer monofilament ε at an arbitrary point Q on the contact surface for a given displacement of the striker d is determined by:

$$\varepsilon = \left(R + h - \sqrt{(R + h - d)^2 + r^2}\right)/h, \qquad (2)$$

where r is the distance between points Q and P on the central axis of the striker. The distribution of strain ε with r for a given displacement of the striker d ($d = 5$ mm) is shown in Figure 9(a). It can be seen that ε changes with r in a parabolic manner. The maximal deformation is located at the central point of the contact surface. The distribution of strain ε with r for various values of d in a cross-section of the fabric through the central axis of the anvil is shown in Figure 9(b). It is clearly seen that all the deformations on the contact surface increase with increase in d. Since the spacer monofilaments within the fabric can deform differently, the plateau stage cannot be observed in the contact force–displacement curves of the fabric under impact in the hemispherical form.

Energy absorption and force attenuation properties

The impact process of the spacer fabric in the hemispherical shape is very complicated. During the impact, the kinetic energy of the striker is transformed into different energy forms, including the energy absorbed by the deformation and damage to the fabric, the energy absorbed by the deformation of the testing system (striker, anvil and supporting mechanism), and the energy lost due to the propagation of stress wave. At the point of maximal deflection and acceleration the total kinetic energy of the striker is completely transformed into deformation energy and the dissipated energy, which include the energy stored by the elastic deformation of the fabric and the testing system, the energy dissipated by the plastic and damage to the fabric and the testing system, and the energy dissipated by the propagation of the stress wave. After this point, the stored energy will transfer to the kinetic energy of the striker, causing the striker to rebound. By neglecting the energy dissipated by the plastic deformation and damage to the testing system, and the energy lost due to the propagation of stress wave, the following energy expressions can be obtained:

$$U_{\text{kinetic}} = U_{\text{elastic}} + U_{\text{elastoplastic}} + U_{\text{damage}} + U_{\text{machine}} \qquad (3)$$

$$U_{\text{mechanical}} = U_{\text{elastic}} + U_{\text{elastoplastic}} \qquad (4)$$

$$U_{\text{residual}} = U_{\text{damage}} + U_{\text{machine}} \qquad (5)$$

where U_{kinetic} is the kinetic energy of the striker, U_{elastic} is the energy stored by elastic deformation of the fabric, $U_{\text{elastoplastic}}$ is the energy absorbed by elastoplastic deformation of the fabric, U_{damage} is the energy dissipated by damage to the filaments, $U_{\text{mechanical}}$ is the energy absorbed by elastic and elastoplastic deformation of the fabric (the area under the contact force–displacement curve, shown in Figure 5), U_{machine} is the energy stored by elastic deformation of the testing system, and U_{residual} is the residual kinetic energy of the striker after being absorbed by the elastic and elastoplastic deformations of the fabric, which need to be dissipated by damage to the fabric (U_{damage}), or transferred to the testing machine (U_{machine}).

Figure 10 shows the energy absorbed by the elastic and elastoplastic deformations of the fabric ($U_{\text{mechanical}}$) against the displacement of the striker at

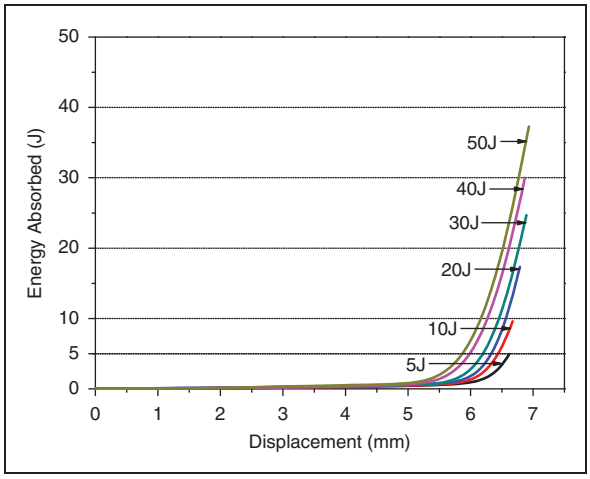

Figure 10. Energy absorbed by the elastic and elastoplastic deformations of the fabric against the displacement of the striker under different impact energies.

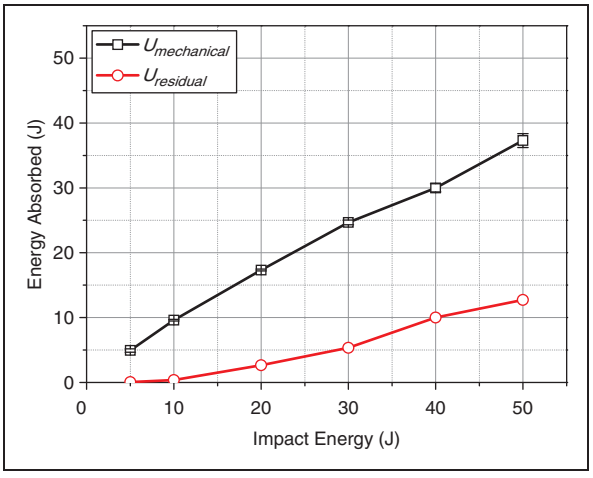

Figure 11. Energy absorbed by the elastic and elastoplastic deformations of the fabric and residual energy for different levels of impact energy.

different levels of impact energy. It can be seen that the absorbed energy increases with increase in impact energy. Since impact by the striker at a higher level of kinetic energy can result in a higher final displacement of the fabric, more energy is absorbed by the fabric due to its greater deformation. Figure 11 shows the energy absorbed by the elastic and elastoplastic deformation of the fabric and the residual energy of the striker. It can be seen that when the impact energy is below 10 J the kinetic energy of the striker is almost completely absorbed by the elastic and elastoplastic deformation of the fabric without heat generation. However, when the impact energy is greater than 10 J, the kinetic energy of the striker cannot be totally absorbed by the elastic and elastoplastic deformation of the fabric, although the energy absorbed by such deformations of the fabric increases as the impact energy increases. In this case, the kinetic energy of the striker not absorbed by elastic and elastoplastic deformation of the fabric is transferred to the residual energy. As shown in Figure 11, the residual energy of the striker also increases as the impact energy increases. When the purely elastic and elastoplastic deformations of the fabric cannot totally absorb the higher kinetic energy of the striker, damage to the filaments takes place. It should be noted that while one part of the residual energy is transformed into heat, the other part together with U_{elastic} and the elastic deformation energy of $U_{\text{elastoplastic}}$ makes the striker rebound.

Figure 12 shows the deformation and damage of the fabric after impact at different levels of impact energy. Severe plastic deformation of the monofilaments in the spacer layer can be observed under lower impact energies (5 J and 10 J). In this case, the monofilaments become kinked, distorted or squashed. Some breakage of the monofilaments is also observed at 10 J impact energy. However, no obvious deformation of the multifilaments is observed in the outer fabric layers. When the impact energy is increased to 20 J, in addition to plastic deformation and breakage of the monofilaments, some breakage of the multifilaments in the outer layers is also observed. When the impact energy reaches 30 J, a hole in the outer upper layer of the fabric is produced by the impact, and at the same time a number of mono- and multifilaments are broken. When the impact energy is 40 J, both mono- and multifilaments are broken and become fused together by the heat generated. When the impact energy reaches 50 J, mono- and multifilaments are broken and become a rigid plastic through a thermoplastic process.

The above analysis shows that the fabric is deformed and damaged in different modes when subject to different impact energies. When the energy absorption capacity of the fabric due to elastic and elastoplastic deformations is higher than the kinetic energy of the striker, the impact energy is totally absorbed by the fabric. In this case, the contact law is determined by the stress–strain nature of the spacer fabric. On the other hand, when the impact energy is higher than the energy absorption capacity due to the elastic and elastoplastic deformations, damage is caused to the fabric as it absorbs the remainder of the kinetic energy of the striker. In this case, the contact law between the striker face and the fabric may change significantly and a very large contact force could be produced, as the striker may collide directly with the anvil.

In the present study no direct collisions occurred between the striker and the anvil, as there were no perforated holes present in the fabrics after impact, as shown in Figure 12. The peak contact force is therefore

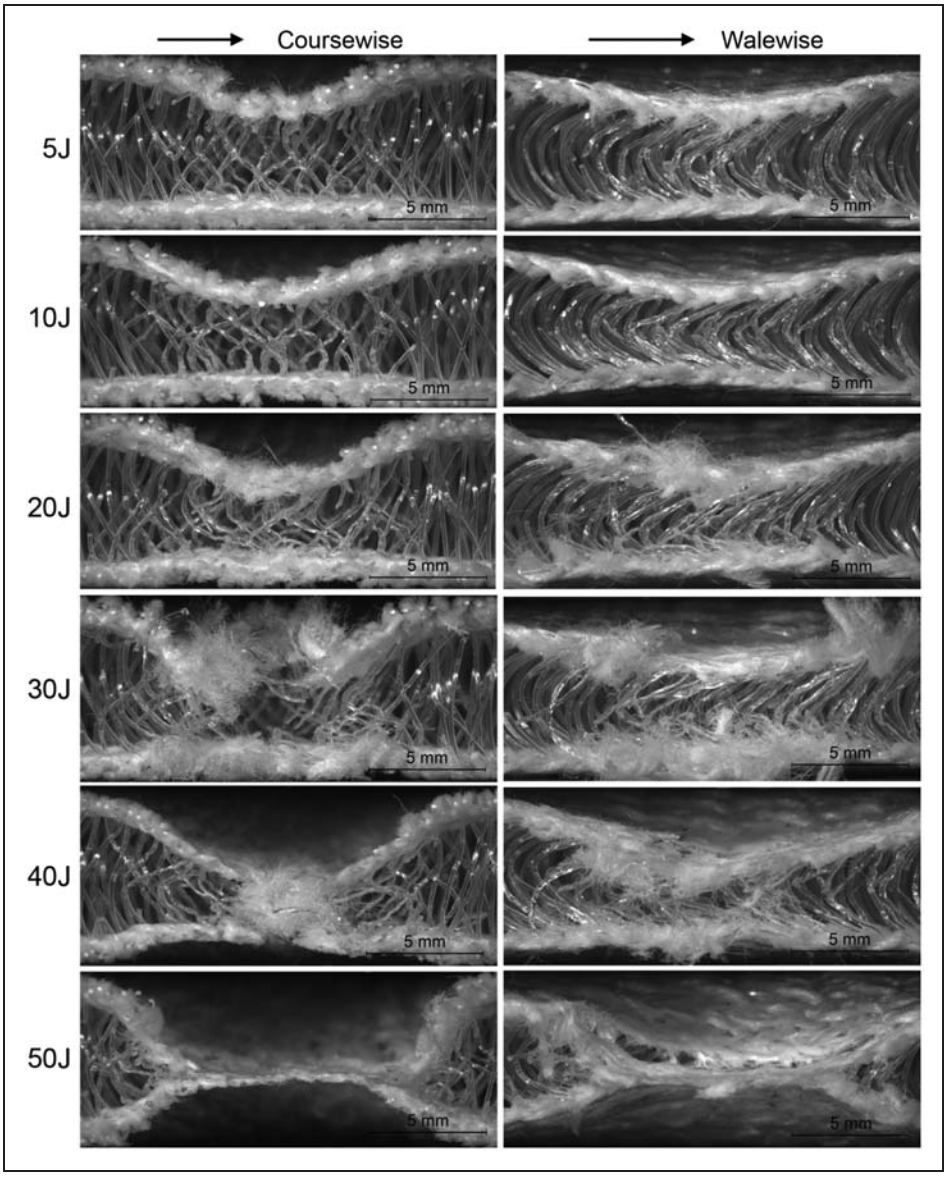

Figure 12. Deformation and damage to the fabric after impact at different levels of impact energy.

determined by the contact stiffness of the compressed fabric at the rebounding point. There is no doubt that a highly densified fabric has a high modulus and therefore a high contact stiffness. Hence, the kinetic energy of the striker is preferably absorbed before the fabric is compressed to its high densification stage.

As mentioned previously, there is a longer plateau stage for the contact force under flatwise impact.[11] This response allows the fabric to absorb a large amount of kinetic energy at a lower constant contact force by elastoplastic deformation. As a result, the spacer fabric possesses superior force attenuation performance under flatwise impact. However, as shown in Figure 5, under impact in the hemispherical form, the contact force curves have a monotonal increasing trend with the displacement, since the spacer monofilaments within the spacer fabric in the hemispherical shape cannot effectively resist the impact load.

To understand the relationship between the force attenuation and the energy absorption behavior of the spacer fabric under impact in the hemispherical form, the energy absorbed by the spacer fabric may be plotted against the contact force, as shown in Figure 13, which indicates that the energy absorbed increases non-linearly with the contact force. Obviously, to absorb more kinetic energy, the spacer fabric must be compressed with a larger displacement into a highly densified stage. This leads to greater contact stiffness, a larger contact area, and a bigger peak contact force between the striker face and the fabric surface. Compared with

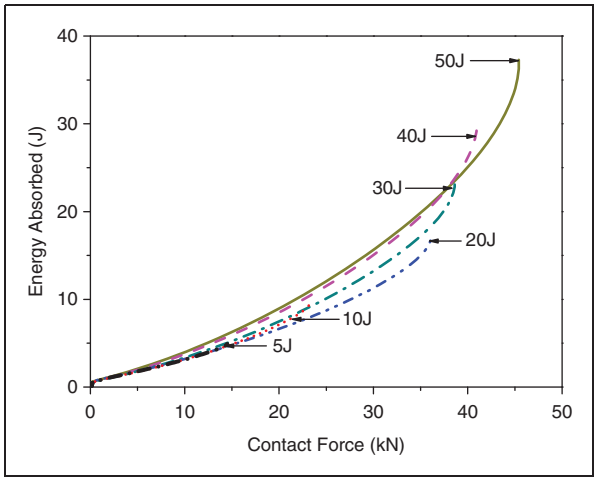

Figure 13. Energy absorbed *versus* contact force at different impact energies.

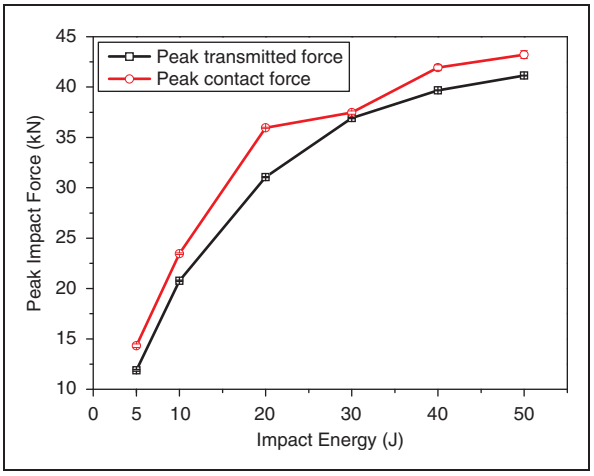

Figure 14. Variations of the peak contact force and peak transmitted force with impact energy.

the impact in the planar shape, the lower efficiency of force attenuation of the spacer fabric in the hemispherical shape is due to the fact that not all of the spacer monofilaments are able to contribute to the resistance to impact loading.

During the impact, the contact force is transmitted to the anvil through the deformed specimen in the form of stress waves. The transmission process is complicated and its mechanism is not relevant to this study. Figure 14 shows the variation in both the peak contact force and the peak transmitted force with impact energy. The results show that both forces increase non-linearly as the impact energy increases. In addition, the peak transmitted force remains below the peak contact force for all impacts. However, the ratio between them is not constant when the impact energy changes. This difference may arise from their different modes of deformation and damage, which can affect the stress wave propagation and damping behavior of the fabric. For instance, for the impact with a kinetic energy of 30 J, the transmitting ratio is higher than those for other impacts. This is the result of a hole created in the top outer fabric layer when many mono- and multifilaments are broken, as can be observed in Figure 12.

According to the European Standard BS EN 1621–1:1998, for motorcyclists' limb impact protectors the mean value of the transmitted forces must not exceed 35 kN and no single value shall exceed 50 kN at an impact energy of 50 J. The test results obtained show that when the impact energy is below 30 J a single layer of the fabric can meet the force transmission requirement. However, when the impact energy is 50 J, as specified in the standard, the transmitted force is 41.14 ± 0.024 kN, which exceeds the value allowed. Due to the severity of motorcycle impacts, a single layer of this particular fabric is thus insufficient to offer adequate protection. In this case, the structure of the fabric should be optimized and lamination employed to enable the protective performance of spacer fabrics to give the required protection. The effect of structural parameters and lamination on protective properties will be discussed in Part II of this paper.

Frequency domain analysis

In order to provide a deeper understanding of the impact behavior of the fabric in the hemispherical shape, a frequency domain analysis was carried out using the Hilbert–Huang transform (HHT) to elucidate the failure mechanisms within the time domain.

Frequency domain analysis methods include fast Fourier transform (FFT), wavelet transform, HHT, etc. The most commonly used method, FFT, is only able to process linear and stationary signals.[13] Wavelet transform can be used for non-stationary signals, but is not applicable to non-linear signals.[14] HHT is a combination of Hilbert spectral analysis and empirical mode decomposition (EMD) to separate a signal into intrinsic mode functions (IMF) and to obtain instantaneous frequency data.[15–17] It is adaptive and highly efficient for analyzing non-linear and non-stationary data in time–frequency–amplitude representation and has been proven to have potential for revealing hidden physical meanings in the data. HHT was therefore adopted here to perform the frequency domain analysis of the transmitted force signals and establish the frequency features that correspond to the deformation and damage modes of the fabric. The analysis was conducted with ensemble EMD (EEMD), which defines

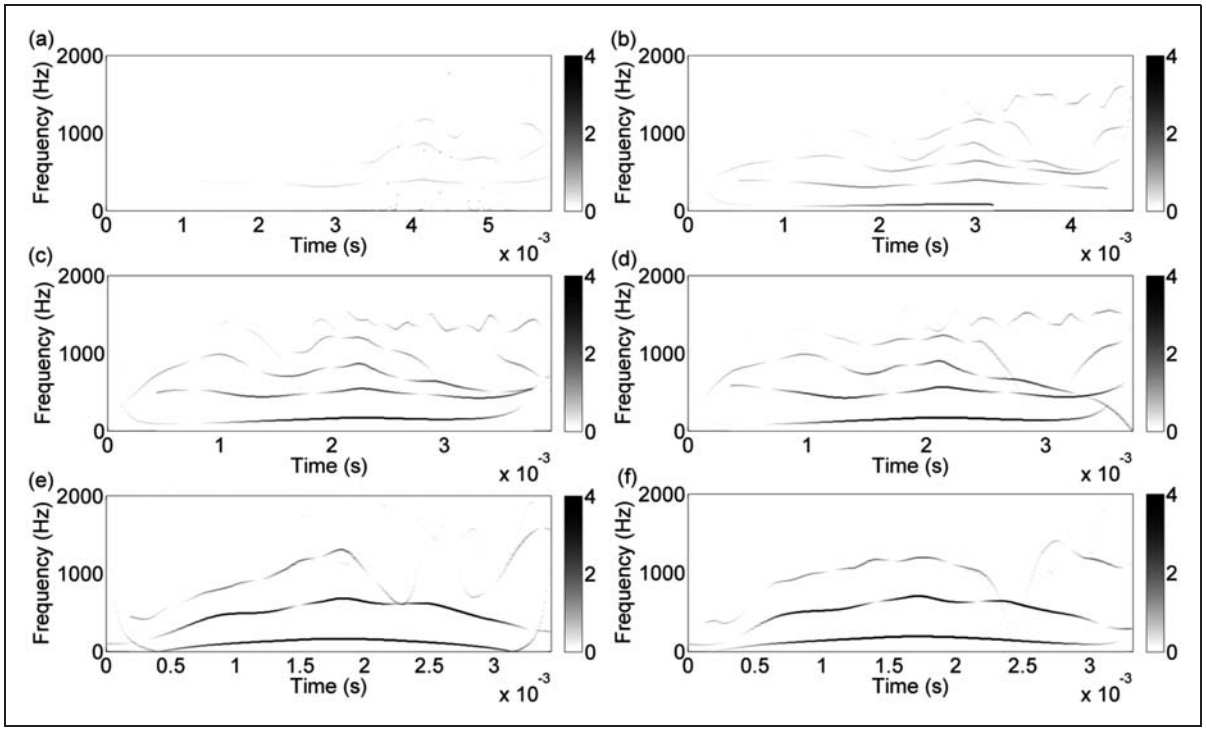

Figure 15. Hilbert spectra for the transmitted force signals obtained from different levels of impact energy: (a) 5 J; (b) 10 J; (c) 20 J; (d) 30 J; (e) 40 J; (f) 50 J.

the IMF components as the mean of an ensemble of trials, each consisting of the signal plus white noise of finite amplitude to prevent mode mixing, and therefore to achieve better results.[18]

The Hilbert spectra for the transmitted force signals obtained at different levels of impact energy are obtained in the time–frequency–amplitude representation shown in Figure 15, providing a measure of amplitude contribution from each frequency and time. The marginal spectrum shown in Figure 16, which provides a measure of the total amplitude contribution from each frequency, is obtained by integrating the Hilbert spectrum in the time domain. From Figure 15, with reference to the transmitted force–time signals (Figure 4(b)), it can be seen that the transmitted force amplitudes are located in different frequency bands. This implies different deformation and damage modes under different levels of impact energy. In addtion, the frequency distribution also varies with time, which indicates that the deformation mode changes during the impact process.

The marginal spectra are always used to identify the deformation and damage modes.[19] The frequency distributions can be divided into a number of ranges, each of which corresponds to a certain deformation or damage mode. There are specific frequency ranges for the plastic deformation of monofilaments,

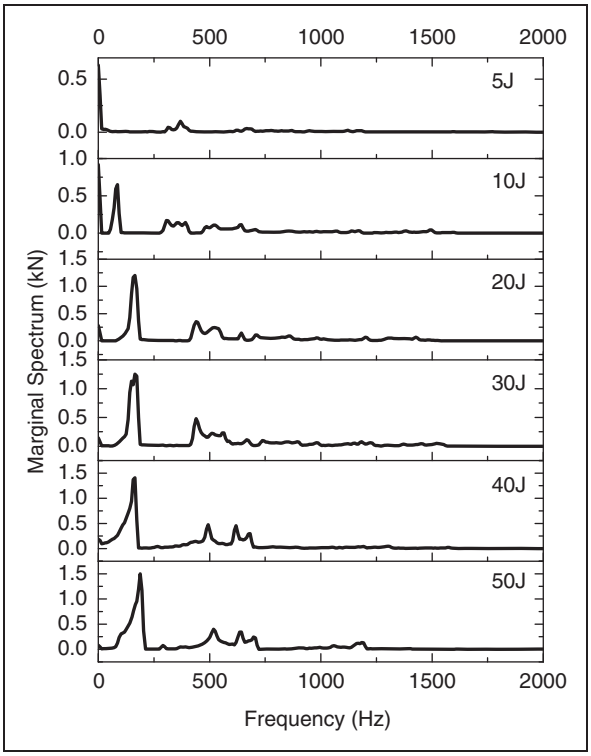

Figure 16. The marginal spectra for the transmitted force signals obtained from different levels of impact energy.

breakages of monofilaments, breakages and thermoplastic transformation of multifilaments. When the frequency ranges have been determined, the related deformation and damage modes can also be determined. By referring to Figure 16 it can be seen that when the impact energy is 5 J the frequencies are located in the ranges 0–10 Hz and 300–425 Hz. However, in addition to these frequency ranges the frequencies distributed in the range 50–100 Hz can also be observed when the impact energy is 10 J. It should be noted that the highest amplitudes are located within the range 0–10 Hz for impact energies of either 5 J or 10 J. The marginal spectra for the impact energy of 20 J and 30 J show a similar frequency pattern, in which the frequencies are distributed in the ranges 0–10 Hz, 80–180 Hz, 400–560 Hz and are concentrated at 164 Hz. For an impact energy of 40 J the frequencies are located in the ranges 0–180 Hz and 400–700 Hz, but are concentrated at 164 Hz. For an impact energy of 50 J the frequencies are located in the ranges 0–210 Hz, 400–700 Hz and are concentrated at 188 Hz.

Based on this analysis, a relationship between the frequency ranges and the deformation and damage modes can be established. It can be speculated that plastic deformation occurs between 0–10 Hz and 300–425 Hz, monofilament breakages occur between 50 and 100 Hz, breakages of multifilaments occur between 80–180 Hz and 400–560 Hz, and the thermoplastic transformation occurs between 180–210 Hz and 560–700 Hz. These results show that the higher the impact energy, the higher the range of the frequency distributed in the marginal frequency spectra. The severe damage to the fabric corresponds to the higher frequency ranges, which are also related to higher transmitted forces. From the frequency domain analysis it is possible to identify deformation and damage modes in the spacer fabric and to evaluate its protective performance when the frequency ranges are known.

Conclusions

A typical warp-knitted spacer fabric developed for human body protection against impact was tested in the hemispherical form at different levels of impact energy. Its impact resistance, energy absorption and force attenuation properties were investigated in the light of the experimental results. The frequency domain analysis with HHT method was also used to analyze its different deformation and damage modes. According to the experimental results and analysis, the following conclusions can be drawn:

1. The boundary condition determines the impact response of the spacer fabric. The plateau stage of the spacer fabric under impact in the hemispherical form is not clearly observed due to the change of the contact area of the fabric during the impact process and different deformation stages of spacer yarns under similar displacement of the striker.
2. The energy absorbed by the fabric depends on the impact energy level. When the impact energy is lower than the energy absorption capacity of the fabric, the impact energy can be totally absorbed by the elastic and elastoplastic deformations of the fabric. However, when the impact energy is higher than the energy absorbed by the elastic and elastoplastic deformation of the fabrics, damage to the fabric cannot be avoided. The severity of the damage of the fabric increases as the impact energy increases. Under impact in the hemispherical form the energy absorption capacity of the fabric is decreased. High curvature of the spacer fabric reduces its energy absorption capability and therefore also its force attenuation properties.
3. The peak contact force of a spacer fabric is determined by its energy absorption capacity and the applied impact kinetic energy. These determine the densified level of the spacer fabric under impact. High densification leads to high contact stiffness, and therefore a high peak contact force. High densification also causes the stress wave to transmit easily and produce a high peak in the transmitted force. A certain level of destruction is helpful to dissipate energy, by decreasing the densification and hence reducing the peak transmitted force.
4. The deformation and damage modes of the fabric under different levels of impact energy can be identified through the frequency domain analysis using the Hilbert–Huang transform method. The higher the impact energy, the higher the frequency range distributed in the marginal spectra.

The effect of fabric structural parameters and lamination on the protective properties of spacer fabrics under impact will be presented in Part II.

Funding

The work was supported by the Innovation and Technology Commission of the Government of the Hong Kong Special Administrative Region, China (ITF project GHP/063/09TP).

References

1. Viano DC, Bir CA, Cheney AK, et al. Prevention of commotio cordis in baseball: an evaluation of chest protectors. *J Trauma* 2000; 49: 1023–1028.
2. Rønning R, Rønning I, Gerner T, et al. The efficacy of wrist protectors in preventing snowboarding injuries. *Am J Sport Med* 2001; 29: 581–585.

3. Lemair M and Pearsall DJ. Evaluation of impact attenuation of facial protectors in ice hockey helmets. *Sports Engineering* 2007; 10: 65–74.
4. Bernhardt DT. Protective sports equipment. In: Hebestreit H and Bar-Or O (eds) *The young athlete*. New York: Wiley, 2008, pp.164–168.
5. Parker MJ, Gillespie WJ and Gillespie LD. Effectiveness of hip protectors for preventing hip fractures in elderly people: systematic review. *BMJ* 2006; 332: 571–574.
6. van Schoor NM, van der Veen AJ, Schaap LA, Smit TH and Lips P. Biomechanical comparison of hard and soft hip protectors, and the influence of soft tissue. *Bone* 2006; 39: 401–407.
7. Laing AC, Feldman F, Jalili M, Tsai CM and Rabinovitch SN. The effects of pad geometry and material properties on the biomechanical effectiveness of 26 commercially available hip protectors. *J Biomech* 2011; 44: 2627–2635.
8. Bellfy PI. Attachment of protective pads for protection of joint surfaces. US Patent 7487557, 2009.
9. Dlugosch S, Hu H and Chan CK. Impact protective clothing in sport: areas of application and level of utilization. *RJTA* 2012; 16: 18–28.
10. Liu YP, Hu H, Zhao L, et al. Compression behavior of warp-knitted spacer fabrics for cushioning applications. *Text Res J* 2012; 82: 11–20.
11. Liu YP, Hu H, Long HR, et al. Impact compressive behavior of warp-knitted spacer fabrics for protective applications. *Text Res J* 2012; 82: 773–788.
12. Guo XF, Long HR and Zhao L. Investigation on the impact and compression-after-impact properties of warp-knitted spacer fabrics. *Text Res J* 2013; 83: 904–916.
13. Walker JS. *Fast Fourier transforms*, 2nd edn. Boca Raton, FL: CRC Press, 1996, p.53.
14. Diniz PSR, Silva EAB and Netto SL. *Digital signal processing: System analysis and design*, 2nd edn. Cambridge: Cambridge University Press, 2010, p.599.
15. Huang NE, Long SR and Shen Z. The mechanism for frequency downshift in nonlinear wave evolution. *Adv Appl Mech* 1996; 32: 59–117.
16. Huang NE, Shen Z, Long SR, Wu MC, Shih HH, Zheng Q, Yen N-C, Tung CC and Liu HH. The empirical mode decomposition and the Hilbert Spectrum for nonlinear and non-stationary time series analysis. *Proc R Soc Lon Ser-A* 1998; 454: 903–995.
17. Huang NE, Shen Z and Long SR. A new view of nonlinear water waves: the Hilbert spectrum. *Annu Rev Fluid Mech* 1999; 31: 417–457.
18. Wu ZH and Huang NE. Ensemble empirical mode decomposition: a noise-assisted data analysis method. *Advances in Adaptive Data Analysis* 2009; 1: 1–41.
19. Yu DJ, Cheng JS and Yang Y. Application of EMD method and Hilbert spectrum to the fault diagnosis of roller bearings. *Mech Syst Signal Pr* 2005; 19: 259–270.